JACS
JOURNAL OF THE AMERICAN CHEMICAL SOCIETY
Article
pubs.acs.org/JACS

Photoluminescent Thermometer Based on a Phase-Transition Lanthanide Silicate with Unusual Structural Disorder

Duarte Ananias,[†] Filipe A. Almeida Paz,[†] Dmitry S. Yufit,[§] Luís D. Carlos,*[,‡] and João Rocha*[,†]

[†]Departments of Chemistry and [‡]Physics, CICECO Aveiro Institute of Materials, University of Aveiro, 3810-193 Aveiro, Portugal
[§]Department of Chemistry, Durham University, South Road, Durham, DH1 3LE, United Kingdom

Supporting Information

ABSTRACT: The hydrothermal synthesis of the novel Na[$LnSiO_4$] (Ln = Gd, Eu, Tb) disordered orthorhombic system is reported. At 100 K, and above, these materials are best described in the centrosymmetric orthorhombic *Pnma* space group. At lower temperatures (structure solved at 30 K) the unit cell changes to body-centered with *Imma* symmetry. The materials exhibit unique photophysical properties, arising from both, this phase transformation, and the disorder of the Ln^{3+} ions, located at a site with D_{2d} point symmetry. $Na[(Gd_{0.8}Eu_{0.1}Tb_{0.1})SiO_4]$ is an unprecedented case of a luminescent ratiometric thermometer based on a very stable silicate matrix. Moreover, it is the first example of an optical thermometer whose performance (viz., excellent sensitivity at cryogenic temperatures <100 K) is determined mainly by a structural transition, opening up new opportunities for designing such devices.

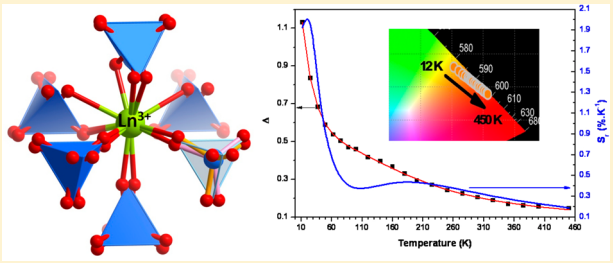

INTRODUCTION

Trivalent lanthanide ions (Ln^{3+}) play a pivotal role in the modern photonic industry due to their exceptional luminescence features, with major applications in phosphors, generation and amplification of light in lasers and optical amplifiers.[1−3] A particularly intriguing use of the Ln^{3+} optical properties is in nonintrusive thermometry based on the decrease of the emission intensity with increasing temperature.[4] In the past decade, a step-forward in the field was the introduction of multicenter Ln^{3+}-based luminescent thermometers containing two rare-earth ions (e.g., Eu and Tb).[4] The emission of each ion exhibits a distinct thermal behavior, and the emission ratio between two specific transitions of the two ions is strongly temperature dependent. These so-called ratiometric thermometers do not present the drawbacks of the thermometers based on single-intensity transition measurements, such as sensor concentration, small material inhomogeneities and optoelectronic drifts of the excitation source and detectors.[2,4,5,4a,b]

Searching for efficient light-emitting materials, we have been interested in new rare-earth silicates, including dense, layered and microporous materials.[5−7] Some of the microporous Ln^{3+} silicates which we have reported display unique and unusual photoluminescence. For example, we have shown that Eu^{3+} photoluminescence spectroscopy is able to identify, at 12 K, enantiomeric domains in $Na_3[(Y,Ln)Si_3O_9]\cdot 3H_2O$,[7b] and that Eu^{3+}-O-Eu^{3+} dimers present in $K_7[Eu_3Si_{12}O_{32}]\cdot xH_2O$ effectively behave as molecular entities embedded in a siliceous matrix.[7c]

The relationship between structural disorder and the photoluminescence properties of bulk lanthanide silicates is still poorly studied. An outstanding example is that of the microporous solid known as AV-20, where besides regular framework Ln(1) ions there are Ln(2) polyhedra disordered over the Na sites (i.e., they statistically occupy the same site), providing an otherwise impossible energy leak.[7d] On the other hand, the detection of phase transitions by Ln^{3+} luminescence is well established, particularly for liquid crystals and to follow structural modification of inorganic materials under high pressures.[8,9]

Here, we wish to report a new lanthanide silicate orthorhombic system, $Na[(Gd_{1-a}Eu_a)SiO_4]$ (a = 0.01, 0.1, 0.4 and 1), exhibiting uncommon photoluminescence properties due to structural disorder and a phase transition. It is also shown that this system constitutes the first example of a ratiometric thermometer based on a Ln^{3+} silicate, particularly sensitive at cryogenic temperatures (<100 K). These materials, which exhibit excellent thermal stability, were prepared under hydrothermal conditions. Despite having the same chemical composition, this system is distinct from the previously reported tetragonal[10] and orthorhombic[11] Na[$LnSiO_4$] materials.

EXPERIMENTAL SECTION

Synthesis of the Materials. The syntheses of rare-earth silicates were carried out in Teflon-lined autoclaves, under static hydrothermal conditions, in ovens preheated at 518 K. The lanthanide nitrate solutions (0.4 M) were prepared by dissolving the corresponding lanthanide oxides (99.99% purity) with stoichiometric amounts of diluted nitric acid under heating. In all the syntheses, the autoclaves

Received: December 15, 2014
Published: February 9, 2015

DOI: 10.1021/ja512745y
J. Am. Chem. Soc. 2015, 137, 3051−3058

were removed and quenched in cold water after an appropriate time. The obtained white microcrystalline powders were filtered out, washed at room temperature with distilled water, and dried at 373 K.

Typical Synthesis of $Na[(Gd_{0.99}Eu_{0.01})SiO_4]$. An alkaline solution was made by mixing 7.01 g of sodium silicate solution (27% m/m SiO_2, 8% m/m Na_2O, Merck), 14.45 g of H_2O and 8.17 g of NaOH (99%, AnalaR Normapur). A mixture of 0.11 mL of $Eu(NO_3)_3$ 0.4 mol·dm^{-3} and 10.89 mL of $Gd(NO_3)_3$ 0.4 mol·dm^{-3} aqueous solutions was added to this solution and stirred thoroughly. The gel, with composition 6.15 Na_2O:1.00 SiO_2:0.121 Gd_2O_3:0.00122 Eu_2O_3:58.5 H_2O, was reacted in Teflon lined autoclaves (volume 37 cm^3) for 5 days at 518 K. $Na[(Gd_{1-a}Eu_a)SiO_4]$ (a = 0.1, 0.4 and 1), $Na[(Gd_{0.8}Tb_{0.1}Eu_{0.1})SiO_4]$ and $Na[(Gd_{0.9}Tb_{0.1})SiO_4]$ samples were synthesized in a similar way, by adjusting the Ln^{3+} amounts (from 0.4 M nitrate solutions) to the desired concentration in the initial gel. To ensure the achievement of the orthorhombic *Pnma* pure samples, ca. 10 mg of a previously synthesized pure phase sample was added to the initial gel as seeds. The synthesis gives ca. 100% yields in terms of the Ln^{3+} inserted in the parent gel, thus the relative concentration of lanthanides in the synthesized product matches that of the initial gel. EDS analysis corroborates this and indicates a homogeneous distribution of the Ln^{3+} ions over the crystals. The morphology and phase purity of all samples have been ascertained by SEM/EDS and powder X-ray diffraction; details are given in the Supporting Information (SI; results in Figures S1, S2 and S3). The compounds are stable up to 1273 K (3 h heating rate of 5 K min^{-1}), Figure S3.

Single-Crystal X-ray Diffraction Studies −100 K. Single-crystals of $Na[(Gd_{0.99}Eu_{0.01})SiO_4]$ were selected in a microscope equipped with a polarized light and were mounted on Hampton Research CryoLoops (using FOMBLIN Y perfluoropolyether vacuum oil (LVAC 140/13) purchased from Sigma-Aldrich).[12] Data were collected at 100(2) K on a Bruker D8 QUEST equipped with Mo Kα sealed tube (Mo Kα, λ = 0.71073 Å), a multilayer TRIUMPH mirror, a PHOTON 100 CMOS detector, and a KRYOFLEX II low-temperature device. The instrument was controlled with the APEX2 software package.[13] Data was processed using the integrate plug-in in the controlling software package (SAINT+),[14] and corrected for absorption by the multiscan semiempirical method implemented in SADABS.[15] The crystal structure was solved using almost all the methods available with the software package. However, due to the presence of heavy atoms, the best approach was using the Patterson synthesis algorithm implemented in SHELXS-97,[16] which allowed the immediate location of most atoms. The remaining atoms were located from difference Fourier maps calculated from successive full-matrix least-squares refinement cycles on F^2 using SHELXL-97.[16a,17] Even though the heaviest atoms in the crystal structure solution of *Pnma* are located in special positions, namely on the mirror plane, the oxygen atoms of the crystallographically independent SiO_4^{4-} tetrahedron are structurally disordered. Consequently, in the overall crystal structure of $Na[(Gd_{0.99}Eu_{0.01})SiO_4]$ the SiO_4^{4-} building unit adopts two distinct crystallographic positions, each with a fixed rate of occupancy of 50%. In this way, the corresponding oxygen atoms were included in the structural model with appropriate fixed rated of occupancy. Even though most of the non-hydrogen atoms were successfully refined with anisotropic displacement parameters, only one pair of disordered oxygen atoms (O2 and O2′) had to be included in the final structural model with a common isotropic thermal displacement parameter. The last difference Fourier map synthesis showed the highest peak (1.338 eÅ^{-3}) and deepest hole (−1.310 eÅ^{-3}) located at 0.81 and 1.10 Å from Na1 and O3, respectively.

Single-Crystal X-ray Diffraction Studies −30 K. Collection of single-crystal X-ray diffraction data at 30 K of material $Na[(Gd_{0.99}Eu_{0.01})SiO_4]$ was carried out on a Bruker D8 VENTURE equipped with Mo Kα high-brilliance IμS radiation (λ = 0.71073 Å), a multilayer X-ray mirror and a PHOTON 100 CMOS detector. Data were collected in three consecutive 170° ω-runs (1° image degree) at different φ setting angles. The low temperature (30 K) was maintained by a Helix (oxford Cryosystems) open-flow helium cryostat. Data was processed using SAINT+,[18] and corrected for absorption by the multiscan semiempirical method implemented in SADABS.[13] The crystal structure was solved using the intrinsic phasing approach implemented in the latest release of SHELXT-2014,[19] which allowed the immediate location of all atoms. At 30 K, the asymmetric unit contains only six atomic positions, of which only atom O2 is in a general position (Wyckoff position 16j). In space group *Imma*, both the Na^+ cation and the tetrahedral SiO_4^{4-} building unit occupy the same average position. In this context, the rates of occupancy for these atoms were fixed at 0.50. Structure refinement was performed in the graphical interface ShelXle[20] using full-matrix least-squares refinement cycles on F^2using the SHELXL.[21] Hydrogen atoms refined successfully using anisotropic displacement parameters. The last difference Fourier map synthesis showed the highest peak (1.231 eÅ^{-3}) and deepest hole (−1.829 eÅ^{-3}) located at 0.63 and 1.10 Å from Na1 and the mixed (Gd1, Eu1) site, respectively. Information concerning crystallographic data collection and structure refinement details is summarized in Table 1. Tables 2 and S1 summarize the most relevant bond distances of the crystallographically independent rare-earth coordination environment determined at 100 K. Tables S2 and S3 list the same structural features for the 30 K crystal structure. Structural drawings have been created using the software package Crystal Impact Diamond.[22] Molecular model units and rotation movies were created using CrystalMaker.[23]

Table 1. Crystal and Structure Refinement Data for Compound $Na[(Gd_{0.99}Eu_{0.01})SiO_4]$ Determined at 100 and 30 K

	100 K	30 K
Formula	$Eu_{0.01}Gd_{0.99}NaO_4Si$	$Eu_{0.01}Gd_{0.99}NaO_4Si$
Formula weight	272.28	272.28
Crystal system	Orthorhombic	Orthorhombic
Space group	*Pnma*	*Imma*
a/Å	6.8161(10)	6.8051(11)
b/Å	5.4758(9)	5.4529(9)
c/Å	9.1617(12)	9.1425(15)
Volume/Å^3	341.95(9)	339.26(10)
Z	4	4
D_c/g cm^{-3}	5.289	5.331
μ(Mo Kα)/mm^{-1}	19.707	19.863
Crystal size/mm	0.012 × 0.010 × 0.002	0.050 × 0.020 × 0.010
Crystal type	Colorless blocks	Colorless blocks
θ range	3.73−27.45	3.73−29.00
Index ranges	$-8 \le h \le 6$	$-9 \le h \le 9$
	$-7 \le k \le 7$	$-7 \le k \le 7$
	$-11 \le l \le 11$	$-12 \le l \le 12$
Reflections collected	3910	2498
Independent reflections	428 [R_{int} = 0.0321]	275 [R_{int} = 0.1165]
Data Completeness	to θ = 27.45°	to θ = 25.24°
	99.1%	100.0%
Final R indices $[I > 2\sigma(I)]^{a,b}$	$R1$ = 0.0210	$R1$ = 0.0311
	$wR2$ = 0.0391	$wR2$ = 0.0610
Final R indices (all data)^{a,b}	$R1$ = 0.0392	$R1$ = 0.0449
	$wR2$ = 0.0446	$wR2$ = 0.0657
Weighting scheme^c	m = 0.0162	m = 0.0243
	n = 1.7333	n = 0.0
Largest diff. peak and hole	1.338 and −1.310 eÅ^{-3}	1.231 and −1.829 eÅ^{-3}

$^a R1 = \Sigma||F_0| - |F_c||/\Sigma|F_0|$. $^b wR2 = (\Sigma[w(F_0^2 - F_c^2)^2]/[w(F_0^2)^2])^{1/2}$. $^c w = 1/[\sigma^2(F_0^2) + (mP)^2 + nP]$ where $P = (F_0^2 + 2F_c^2)/3$.

Crystallographic data (excluding structure factors) for the crystal structure of $Na[(Gd_{0.99}Eu_{0.01})SiO_4]$ have been deposited with the ICSD as supplementary publication nos. CSD-427288 (at 100 K) and CSD-427992 (at 30 K). Further details of the crystal structure investigation may be obtained from Fachinformationszentrum Karlsruhe, 76344 Eggenstein-Leopoldshafen, Germany (fax:

DOI: 10.1021/ja512745y
J. Am. Chem. Soc. 2015, 137, 3051−3058

Table 2. Bond Distances (in Å) for the Crystallographically Independent Lanthanide Metal Center Coordination Polyhedron Present in $Na[(Gd_{0.99}Eu_{0.01})SiO_4]$ at 100 K[a,b]

Ln1−O2′^{i}	2.264(10)	Ln1−O3^{vi}	2.418(6)
Ln1−O2′^{ii}	2.264(10)	Ln1−O3^{vii}	2.418(6)
Ln1−O2	2.308(10)	Ln1−O2′	2.538(9)
Ln1−O2^{iii}	2.308(10)	Ln1−O2′^{iii}	2.538(9)
Ln1−O1^{iv}	2.365(6)	Ln1−O3^{iv}	2.551(6)
Ln1−O1^{v}	2.365(6)	Ln1−O3^{v}	2.551(6)
Ln1−O2^{i}	2.410(10)	Ln1−O1^{viii}	2.687(6)
Ln1−O2^{ii}	2.410(10)	Ln1−O1^{ix}	2.687(6)

[a]Symmetry transformations used to generate equivalent atoms: (i) $-1/2 + x, 1/2 - y, 1/2 - z$; (ii) $-1/2 + x, y, 1/2 - z$; (iii) $x, 1/2 - y, z$; (iv) $-x, -1/2 + y, 1 - z$; (v) $-x, 1 - y, 1 - z$; (vi) $1/2 - x, -1/2 + y, -1/2 + z$; (vii) $1/2 - x, 1 - y, -1/2 + z$; (viii) $x, 3/2 - y, z$; (ix) $x, -1 + y, z$. [b]$Ln^{3+} = (Gd_{0.99}Eu_{0.01})^{3+}$.

(+49)7247−808−666; e-mail: crysdata@fiz-karlsruhe.de, http://www.fizkarlsruhe.de/request_for_deposited_data.html) on quoting the appropriate CSD number.

Photoluminescence. The emission and excitation spectra were recorded using a Fluorolog-2 Horiba Scientific (Model FL3−2T) spectroscope, with a modular double grating excitation spectrometer (fitted with a 1200 grooves/mm grating blazed at 330 nm) and a TRIAX 320 single emission monochromator (fitted with a 1200 grooves/mm grating blazed at 500 nm, reciprocal linear density of 2.6 nm.mm-1), coupled to a R928 Hamamatsu photomultiplier, using the front face acquisition mode. The excitation source was a 450 W Xe arc lamp. The emission spectra were corrected for detection, and optical spectral response of the spectrofluorometer and the excitation spectra were corrected for the spectral distribution of the lamp intensity using a photodiode reference detector. Time-resolved measurements have been carried out using a 1934D3 phosphorimeter coupled to the Fluorolog-3, and a Xe−Hg flash lamp (6 μs/pulse half width and 20−30 μs tail) was used as the excitation source. The variable temperature measurements were performed using a helium-closed cycle cryostat with vacuum system measuring ca. 10^{-6} mbar and a Lakeshore 330 autotuning temperature controller with a resistance heater. The temperature can be adjusted from ca.12 to 450 K.

RESULTS AND DISCUSSION

Crystallographic Studies. At 100 K, $Na[(Gd_{0.99}Eu_{0.01})SiO_4]$ crystallizes in the centrosymmetric orthorhombic space group *Pnma* (Table 1).

The three crystallographically independent heaviest atoms are located on the mirror plane of the unit with a Wyckoff position of *4c*. This is particularly relevant in the structural description, and in the understanding of the photophysical properties arising from the mixed-lanthanide Gd1, Eu1 site whose coordination geometry is best described as a distorted dodecahedron with approximate D_{2d} point symmetry (Figure 1). As depicted in Figure 1 (100 K structure) the structural disorder associated with the tetrahedral SiO_4^{4-} building unit results in a multitude of local coordination environments with subtle differences in the first coordination sphere (see geometrical data in Tables 2 and S1 in the SI). This dispersion of bond lengths and angles arises as the main justification for the observation of various, almost similar, local coordination environments for Eu^{3+} (see photoluminescence studies below).

At lower temperatures this structural disorder seems to fade away. A structural determination at 30 K reveals the crystal symmetry to increase, being best described as a body-centered unit cell with overall symmetry *Imma* (Table 1). With this symmetry the disordered tetrahedral SiO_4^{4-} building unit and the charge-balancing Na^+ cation occupy in the unit cell almost the same average crystallographic position; these units were included in the structural model with a 50% fixed rate occupancy (see technical section for additional details). Because of the higher symmetry, the coordination polyhedron of mixed-lanthanide Gd1, Eu1 at 30 K seems to be 16-coordinated (see video in the SI). However, if one takes into account the various site occupancy factors the overall coordination geometry remains similar to that determined at 100 K (with an approximate D_{2d} point symmetry; Figure 1, bottom).

At 30 K the disorder around the rare-earth site is, nevertheless, drastically reduced: the coordination dodecahedron only contains one average coordination position belonging to disordered oxygen atoms, contrasting with seven for the crystal structure determination at 100 K. This feature arises from a reduction of the structural disorder associated with the tetrahedral SiO_4^{4-} unit which, at 30 K, has a single oxygen atom disordered over two distinct crystallographic positions (Figure 1, bottom).

Irrespective of the temperature, the crystal structure of $Na[(Gd_{0.99}Eu_{0.01})SiO_4]$ is very dense, with the charge-balancing Na^+ cations fully occupying the available space in the lanthanide silicate network (Figure 2; structure at 100 K). Indeed, upon reducing the temperature from 100 to 30 K the total volume of the unit cell only contracts by ca. 0.76%, a value that is a clear indication of the densely packing of individual chemical moieties. Moreover, the crystal packing seems to be mainly driven by the distribution and connectivity between the lanthanide cations, leading to a diamond-type network whose topological representation is given in Figure 3. Even though the interlanthanide connections in this topology [3.5349(8) and 4.5568(9) Å at 100 K] are ensured by the tetrahedral SiO_4^{4-} building units, their disorder does not influence the overall connectivity. This structural feature is the most likely explanation for this unusual structural disorder of the SiO_4^{4-} building units at 100 K, which is significantly reduced at 30 K.

Photoluminescence Spectroscopy. The photoluminescence properties lend support to the structural disorder in $Na[(Gd_{0.99}Eu_{0.01})SiO_4]$ indicated by the X-ray diffraction studies. Because the simulated (100 K) and experimental (296 K) powder X-ray diffraction patterns of $Na[(Gd_{0.99}Eu_{0.01})SiO_4]$ are similar (Figure S2 in the SI), we assume that no significant structural changes occur in the 100−296 K range. Thus, all spectroscopic results recorded at 296 K pertain to the *Pnma* structure. The excitation spectrum of $Na[(Gd_{0.99}Eu_{0.01})SiO_4]$ (Figure S4 in the SI) shows the typical $^7F_0 \rightarrow {}^5D_{0-4}$, $^5L_6$, $^5G_{2-6}$, $^5H_{3-7}$ and $^5F_{1-5}$ Eu^{3+} intra4f^6 transitions. The appearance of the $^8S_{7/2} \rightarrow {}^6P_{5/2,\,7/2}$ and $^6I_{9/2,\,11/2,\,13/2}$ Gd^{3+} intra4f^7 transitions is due to an effective Gd^{3+}-to-Eu^{3+} energy transfer. Additionally, the partial broad band at higher energy can presumably be attributed to a O^{2-}(2p)-to-Eu^{3+} charge transfer excitation.

The 296 K emission spectrum shows the typical narrow lines ascribed to the Eu^{3+} $^5D_0 \rightarrow {}^7F_{0-4}$ transitions (Figure 4). The strong prevalence of the $^5D_0 \rightarrow {}^7F_4$ transition indicates the presence of the Eu^{3+} ions in a highly polarizable coordination environment with local symmetry corresponding to a coordination polyhedron slightly distorted from the D_{2d} as indicated by X-ray diffraction.[24] Moreover, the two $^5D_0 \rightarrow {}^7F_0$ transitions (Figure 4, inset a) and the local-field splitting of the $^7F_1$ level in at least four Stark components (Figure 4, inset b) indicate the presence of multiple Eu^{3+} local sites brought about by the structural disorder.

DOI: 10.1021/ja512745y
J. Am. Chem. Soc. 2015, 137, 3051−3058

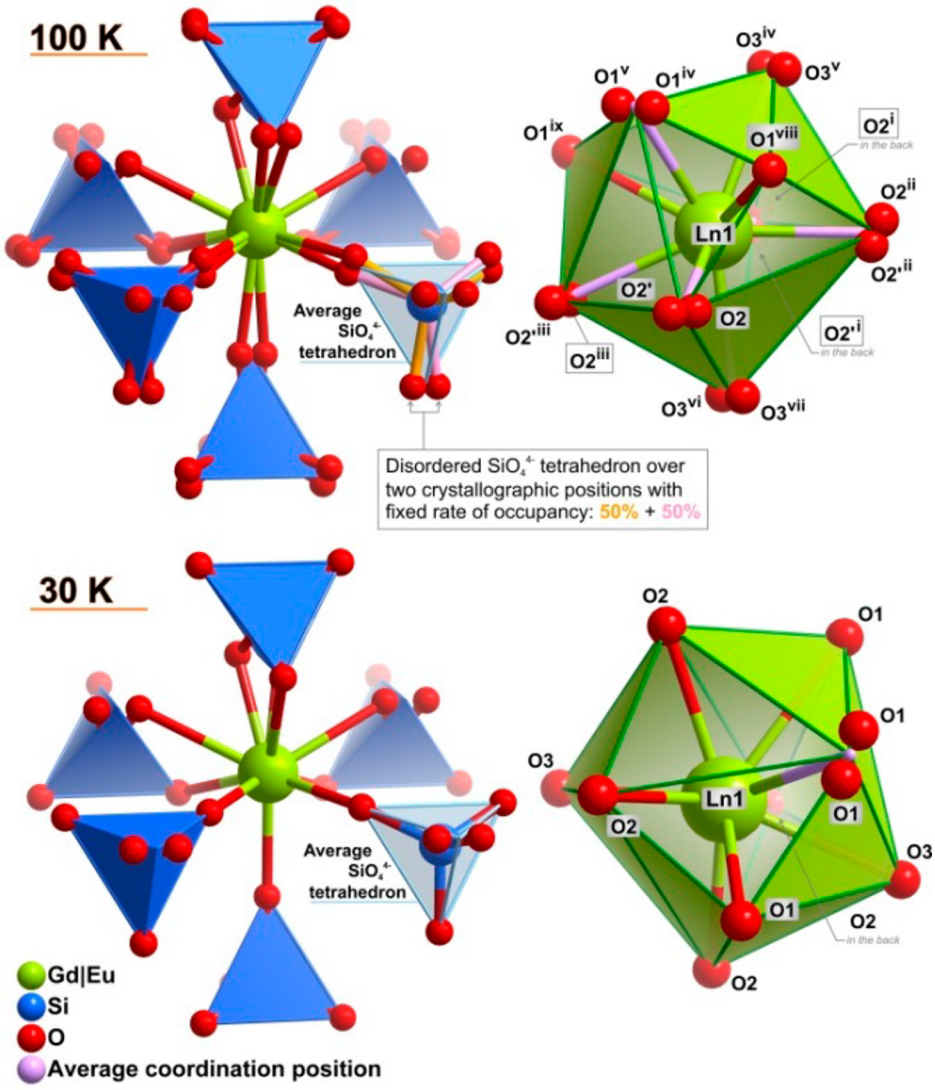

Figure 1. (Left) Schematic representation of the coordination environment of the mixed-lanthanide site present in the crystal structure of $Na[(Gd_{0.99}Eu_{0.01})SiO_4]$ at 100 and 30 K, emphasizing the highly disordered nature of the six symmetry-related coordinating SiO_4^{4-} tetrahedral units. (Right) First coordination sphere of the mixed-lanthanide Ln1 site showing the distorted dodecahedral coordination geometry considering the average coordinating positions of the disordered oxygen atoms. For bond lengths and angles referring to the mixed-lanthanide Ln1 coordination sphere see Tables 2 (100 K), S2 (100 K) and S3–S4 (30 K) in the SI. Symmetry transformations used to generate equivalent atoms for the crystal structure determination at 100 K: (i) $-1/2 + x, 1/2 - y, 1/2 - z$; (ii) $-1/2 + x, y, 1/2 - z$; (iii) $x, 1/2 - y, z$; (iv) $-x, -1/2 + y, 1 - z$; (v) $-x, 1 - y, 1 - z$; (vi) $1/2 - x, -1/2 + y, -1/2 + z$; (vii) $1/2 - x, 1 - y, -1/2 + z$; (viii) $x, 3/2 - y, z$; (ix) $x, -1 + y, z$. Symmetry codes for the equivalent atoms of the structure at 30 K have been omitted for clarity.

The structural modifications mentioned in the crystallographic section are also revealed by Eu^{3+} photoluminescence. Indeed, the temperature changes observed in the $^5D_0 \rightarrow {}^7F_1$ region (Figure 5), are strong evidence for the $Na[(Gd_{0.99}Eu_{0.01})SiO_4]$ transition from the *Pnma* to *Imma* space groups. For instance, the relative intensity of the $^7F_1$ Stark components remains essentially constant from 296 to 100 K and shows a strong variation at 30 K and below (Figure 5).

The 12 K emission spectra recorded with selective excitation (Figure S5 in the SI) display, at least, eight distinct emission lines in the $^5D_0 \rightarrow {}^7F_1$ transition region and, thus, more than three low symmetry Eu^{3+} local sites. This shows that crystal disorder is still present at 12 K. Moreover, the emission lines at 588.0, 589.2, and 589.9 nm have an independent response to the excitation wavelength (Figure S6 in SI) and, thus, are ascribed to distinct Eu^{3+} local sites.

The corresponding $^5D_0$ decay curves (inset in Figure S5 in the SI), independently of the excitation and emission wavelengths, are always fitted by a first-order exponential function giving a lifetime value of 2.50 ± 0.03 ms. Identical Eu^{3+} emission lifetime values correspond to similar environments, which in the present system is justified by structural disorder.

It could be argued that the presence of several Eu^{3+} local sites is due to impurities or defects present in $Na[(Gd_{0.99}Eu_{0.01})SiO_4]$. This is not the case because the 296 K emission spectra of a series of $Na[(Gd_{1-a}Eu_a)SiO_4]$ (a = 0.01, 0.2, 0.4, 1.0) samples (Figure S7 in the SI) are similar. However, increasing the Eu^{3+} loading increases the energy migration between metal ions, thus, decreasing the $^5D_0$ lifetimes (Figure S8 in the SI).

Ratiometric Thermometer. Next, sample $Na[(Gd_{0.8}Eu_{0.1}Tb_{0.1})SiO_4]$ was assessed as a ratiometric ther-

DOI: 10.1021/ja512745y
J. Am. Chem. Soc. 2015, 137, 3051–3058

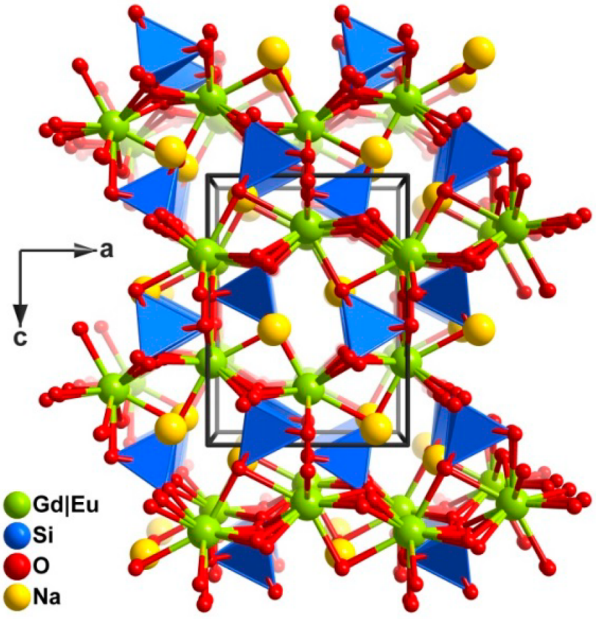

Figure 2. Mixed ball-and-stick and polyhedra representation (only for the average position of the SiO_4^{4-} tetrahedron) of the crystal packing of $Na[(Gd_{0.99}Eu_{0.01})SiO_4]$ at 100 K, viewed along the [010] direction of the unit cell.

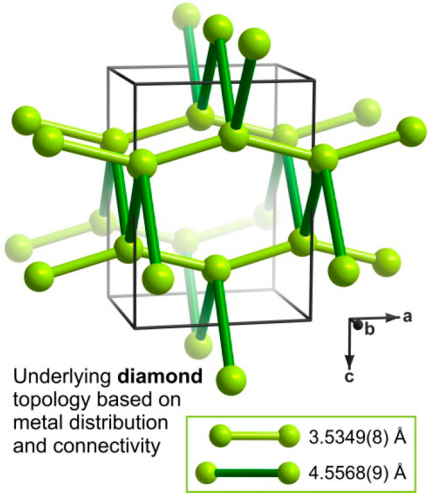

Figure 3. Simplification of the crystal structure of $Na[(Gd_{0.99}Eu_{0.01})SiO_4]$ at 100 K emphasizing the underlying diamond-type network established by the metallic centers and their shortest intermetallic distances along the [100] and [010] directions of the unit cell.

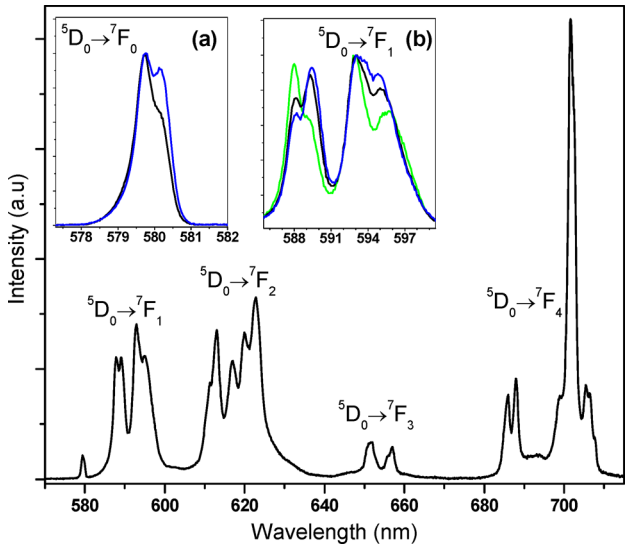

Figure 4. Emission spectra of $Na[(Gd_{0.99}Eu_{0.01})SiO_4]$ acquired at 296 K with excitation at 393 nm. The inset (a) shows the $^5D_0 \rightarrow {}^7F_0$ region while exciting the sample at 393.0 nm (black line) and 393.5 nm (blue line); inset (b) shows the $^5D_0 \rightarrow {}^7F_1$ region with selective excitation at 392.5 (green line), 393.0 (black line) and 393.5 (blue line). These excitation wavelengths have been chosen according with the excitation spectra in the inset of Figure S4 in the SI.

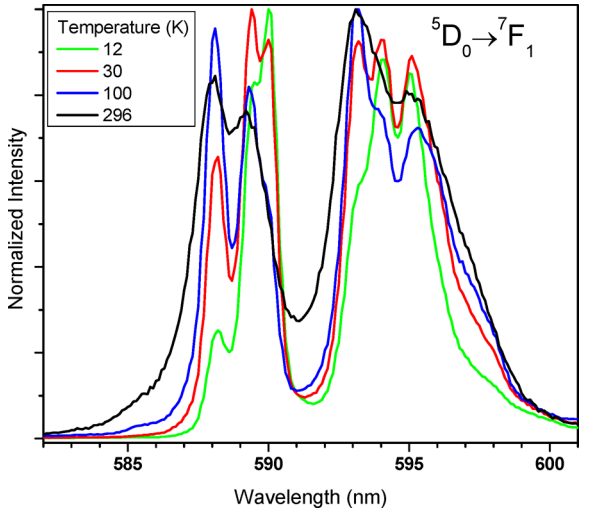

Figure 5. Temperature dependence of the $Na[(Gd_{0.99}Eu_{0.01})SiO_4]$ emission spectra in the $^5D_0 \rightarrow {}^7F_{0,1}$ transitions region. The excitation was fixed at 393 nm.

mometer. This material presents both Gd^{3+}-to-Eu^{3+}, Gd^{3+}-to-Tb^{3+} and Tb^{3+}-to-Eu^{3+} energy transfer, which depends on the temperature, as shown by the excitation spectra recorded at 296 and 12 K (Figure S9 in the SI). For comparison purposes, we also provide the 296 K excitation spectrum of $Na[(Gd_{0.9}Tb_{0.1})SiO_4]$ (Figure S10 in the SI). For $Na[(Gd_{0.8}Eu_{0.1}Tb_{0.1})SiO_4]$, upon Tb^{3+} excitation at 483 nm ($^7F_6 \rightarrow {}^5D_4$ transition), the emission spectra (Figure 6a) present both the Tb^{3+} ($^5D_4 \rightarrow {}^7F_{5-0}$) and Eu^{3+} ($^5D_0 \rightarrow {}^7F_{0-4}$) transitions, whose relative intensities depend on the temperature. Increasing the temperature promotes the Tb^{3+}-to-Eu^{3+} energy transfer, with concomitant evolution of the emission color from yellow at 12 K (Tb^{3+} plus Eu^{3+} emissions) to red (essentially Eu^{3+} emission), as shown in the CIE (Commission Internationale de l'Eclairage) chromaticity diagram (Figure S11 in the SI).

The absolute temperature measurement is inferred via the experimental parameter Δ,[25a] defined here as the integrated intensity ratio of the $^5D_4 \rightarrow {}^7F_5$ (Tb^{3+}) and $^5D_0 \rightarrow {}^7F_4$ (Eu^{3+}) transitions. Another example of a Eu^{3+}/Tb^{3+} ratiometric thermometer involving the $^5D_0 \rightarrow {}^7F_4$ transition was reported very recently by Wu et al.[25b] It is an added value of the present thermometer the fact that this line does not overlap with any Tb^{3+} lines, while its abnormal intensity (by reference to most Eu^{3+} compounds) is due to the presence of Eu^{3+} ions in a coordination polyhedron slightly distorted from the D_{2d} point group.[24] The temperature dependence of the Δ parameter may be described by the classical Mott–Seitz model involving two

DOI: 10.1021/ja512745y
J. Am. Chem. Soc. 2015, 137, 3051−3058

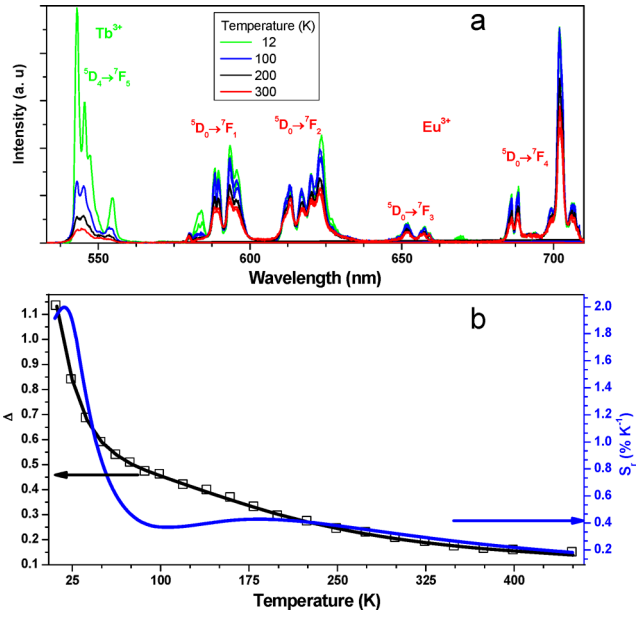

Figure 6. (a) Emission spectra of $Na[(Gd_{0.8}Eu_{0.1}Tb_{0.1})SiO_4]$ as a function of temperature under 483.5 nm excitation. (b) Ratiometric intensity parameter Δ as a function of temperature, for $Na[(Gd_{0.8}Eu_{0.1}Tb_{0.1})SiO_4]$ and corresponding temperature sensitivity (S_r; blue line). The black line represents the calibration curve obtained by the best fit of the experimental points to eq 1 ($r^2 > 0.999$).

nonradiative recombination channels in competition (see details in the SI):[26]

$$\Delta(T) = \frac{\Delta_0}{1 + \alpha_1 \exp(-\Delta E_1/k_B T) + \alpha_2 \exp(-\Delta E_2/k_B T)} \quad (1)$$

where Δ_0 is the Δ parameter at $T = 0$ K, $\alpha = W_0/W_R$ is the ratio between the nonradiative (W_0 at $T = 0$ K) and radiative (W_R) rates, and ΔE_1 and ΔE_2 are the activation energies for the two nonradiative channels. The black line in Figures 6b and S12 in SI represent the temperature calibration curve, obtained by fitting the experimental points to eq 1, yielding $\Delta_0 = 1.21$, $\alpha_1 = 2.47$, $\alpha_2 = 20.7$, $\Delta E_1 = 29.8$ cm^{-1} and $\Delta E_2 = 418$ cm^{-1}; T is the absolute temperature. According to the excitation spectra (296 and 12 K) of $Na[(Gd_{0.8}Eu_{0.1}Tb_{0.1})SiO_4]$ (Figure S9 in the SI), the nonradiative recombination channel characterized by the activation energy ΔE_2 involves the Eu^{3+} $^5D_2$ level (Tb^{3+}-to-Eu^{3+} energy transfer, see below). The much smaller activation energy ΔE_1 probably involves nonradiative deactivations through the multiple Tb^{3+} local sites (and, thus, the multiple resonant $^5D_4$ levels) brought about by the structural disorder (Tb^{3+}-to-Tb^{3+} energy migration, see details in the SI). The calculated temperature relative sensitivity, $S_r = (\partial\Delta/\partial T)/\Delta$,[27] is also plotted in Figure 6b for temperatures between 12 and 450 K. Presumably due to the temperature phase transition (ca. 100 to 30 K, see above) two regimes of temperature sensing are observed, one from 12 to ca. 100 K (S_r decreasing from ca. 2.0 to 0.35% K^{-1}) and a second regime between 100 and 450 K (S_r decreasing from 0.35 to 0.10% K^{-1}). Close to room temperature, the relative sensitivity is ca. 0.36% K^{-1}, a value slightly lower than the values reported for ratiometric thermometers based on Ln^{3+} upconversion nanoparticles.[28,29] Thus, $Na[(Gd_{0.8}Eu_{0.1}Tb_{0.1})SiO_4]$ is a very sensitive photoluminescent ratiometric thermometer for the cryogenic temperature range, e.g., $S_r = 1.0\%\cdot K^{-1}$ at 50 K. This material outperforms other luminescent thermometers, for example, the Eu/Tb bearing metal−organic frameworks reported by Cui et al.[4h] and Vries et al.,[4i] whose relative sensitivities are, respectively, 0.42 and 0.62%·K^{-1}, at 50 K. Cryogenic temperature sensing is crucial for many research and industrial applications, namely in the energy and aerospace industries. Although the sensitivity of other optical techniques, such as Rayleigh backscattering spectral shift by optical frequency-domain reflectometry may be as high as $S_r = 9\%\cdot K^{-1}$ at 77.6 K (with uncertainly of 0.3 K), this is a sophisticated and expensive technique operative only at meter length scales above 77 K, also requiring a complex data analysis.[30]

Temperature cycling shows repeatability readout better than 98% (Figure S14 in the SI illustrates this for the range 12−400 K). Moreover, converting the time fluctuations of the thermometric parameter Δ into temperature, the uncertainty of the temperature measurement is 1.2 K at room temperature (Figure S15 in the SI).

The temperature sensing capability of the ratiometric $Na[(Gd_{0.9}Eu_{0.1}Tb_{0.1})SiO_4]$ thermometer is due to the temperature dependence of the Tb^{3+}-to-Eu^{3+} energy transfer, occurring mainly via the dipole−quadrupole and quadrupole−quadrupole mechanisms.[31a] Considering a Föster-type multipolar mechanism, the efficiency, η_{ET}, and probability, k_{ET}, of the Tb^{3+}-to-Eu^{3+} energy transfer may be determined from the experimental donor (Tb^{3+}) lifetime in the presence (τ_{DA}) and in the absence of the acceptor (Eu^{3+}; τ_D):[6a,31]

$$\eta_{ET} = 1 - \tau_{DA}/\tau_D \quad (2)$$

$$k_{ET} = \tau_{DA}^{-1} - \tau_D^{-1} \quad (3)$$

Considering the $^5D_4$ lifetimes measured in the presence and absence of the acceptor, respectively $Na[(Gd_{0.8}Eu_{0.1}Tb0_{0.1})SiO_4]$ and $Na[(Gd_{0.9}Tb_{0.1})SiO_4]$ (Figure 7), an energy-transfer efficiency and probability of, respectively, 22% and 115 s^{-1} at 12 K and 62% and 691 s^{-1} at 296 K, are obtained. Because the 296 K $^5D_4$ decay curve is biexponential, the τ_{DA} value considered is an average. In contrast, at 12 K the decay curve is monoexponential. This different behavior with temperature is ascribed to both, the *Pnma* to *Imma* phase transition, and the decrease in the local Ln^{3+} disorder, revealed by X-ray diffraction. We note that the $^5D_0$ decay curves of $Na[EuSiO_4]$ exhibit a similar behavior (Figure S8).

CONCLUSIONS

A new lanthanide silicate orthorhombic system, $Na[LnSiO_4]$ (Ln = Gd, Eu, Tb), exhibiting unusual structural disorder, was presented. The centrosymmetric *Pnma* crystal structure, stable at 100 K and above, undergoes a phase transition to a body-centered unit cell in the *Imma* space group (measured at 30 K). This transition reduces, but does not eliminate, the structural disorder. The very unusual Ln^{3+} D_{2d} point symmetry is maintained in both structures originating the predominance of the Eu^{3+} $^5D_0 \rightarrow {}^7F_4$ emission. Photoluminescence also reveals the presence of structural disorder providing evidence for multiple and spectroscopically very similar Eu^{3+} local sites. The phase transition is witnessed by the changes in the relative intensities of the $^5D_0 \rightarrow {}^7F_1$ lines. The introduction of Tb^{3+} and Eu^{3+} ions (sample $Na[(Gd_{0.8}Eu_{0.1}Tb_{0.1})SiO_4]$) affords an unprecedented example of a photoluminescent ratiometric thermometer based on a robust and very stable silicate matrix. The fact that this noncontact sensor is very sensitive at cryogenic temperatures (<100 K) is ascribed to both the phase

DOI: 10.1021/ja512745y
J. Am. Chem. Soc. 2015, 137, 3051−3058

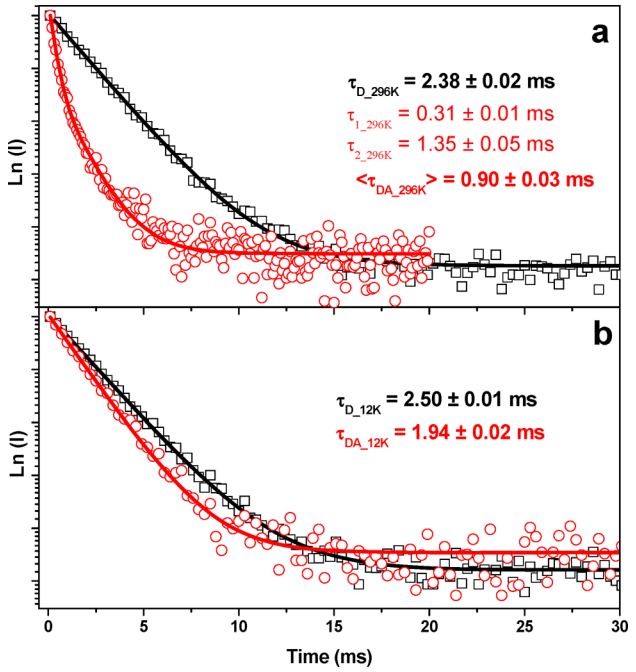

Figure 7. $^5D_4$ decay curves of $Na[(Gd_{0.9}Tb_{0.1})SiO_4]$ (black) and $Na[(Gd_{0.8}Eu_{0.1}Tb_{0.1})SiO_4]$ (red) recorded at 296 K (a) and at 12 K (b), with excitation at 483.5 nm and emission at 543 nm. The lines are the best fits using first-order ($I = I_0 + A_1e^{-x/\tau}$) and second-order ($I = I_0 + A_1e^{-x/\tau_1} + A_2e^{-x/\tau_2}$) decay functions ($r^2 > 0.99$). The average lifetime, $\langle\tau\rangle$, is defined as $(A_1\tau_1^2 + A_2\tau_2^2)/(A_1\tau_1 + A_2\tau_2)$.[32]

transition and the decrease in the local Ln^{3+} disorder at such temperatures, with the former probably prevailing. To the best of our knowledge, this is the first example of a luminescence thermometer whose performance is determined mainly by a structural transition, opening up new avenues for designing such devices.

■ ASSOCIATED CONTENT

Supporting Information

Details and additional characterization such as SEM images, powder X-ray diffraction at ambient temperature and PL. This material is available free of charge via the Internet at http://pubs.acs.org.

■ AUTHOR INFORMATION

Corresponding Authors

lcarlos@ua.pt
rocha@ua.pt

Notes

The authors declare no competing financial interest.

■ ACKNOWLEDGMENTS

This work was developed in the scope of the project CICECO-Aveiro Institute of Materials (Ref. FCT UID/CTM/50011/2013), financed by national funds through the FCT/MEC and when applicable co-financed by FEDER under the PT2020 Partnership Agreement. D.A. acknowledges FCT for Postdoc Grant SFRH/BPD/95032/2013.

■ REFERENCES

(1) (a) Feldmann, C.; Jüstel, T.; Ronda, C. R.; Schmidt, P. J. *Adv. Funct. Mater.* **2003**, *13*, 511−516. (b) Eliseeva, S. V.; Bünzli, J.-C. G. *Chem. Soc. Rev.* **2010**, *39*, 189−227.

(2) Werts, M. H. V. *Sci. Prog.* **2005**, *88*, 101−131.

(3) Polman, A.; van Veggel, F. C. J. M. *J. Opt. Soc. Am. B* **2004**, *21*, 871−892.

(4) (a) Carlos, L. D.; Ferreira, R. A. S.; Rainho, J. P. *Adv. Funct. Mater.* **2002**, *12*, 819−823. (b) Brites, C. D. S.; Lima, P. P.; Silva, N. J. O.; Millán, A.; Amaral, V. S.; Palacio, F.; Carlos, L. D. *Adv. Mater.* **2010**, *22*, 4499−4504. (c) Brites, C. D. S.; Lima, P. P.; Silva, N. J. O.; Millan, A.; Amaral, V. S.; Palacio, F.; Carlos, L. D. *New J. Chem.* **2011**, *35*, 1177−1183. (d) Rao, X.; Song, T.; Gao, J.; Cui, Y.; Yang, Y.; Wu, C.; Chen, B.; Qian, G. *J. Am. Chem. Soc.* **2013**, *135*, 15559−15564. (e) Vetrone, F.; Naccache, R.; Zamarron, A.; de la Fuente, A. J.; Sanz-Rodriguez, F.; Maestro, L. M.; Rodriguez, E. M.; Jaque, D.; Solé, J. G.; Capobianco, J. A. *ACS Nano* **2010**, *4*, 3254−3258. (f) Peng, H. S.; Stich, M. I. J.; Yu, J. B.; Sun, L. N.; Fischer, L. H.; Wolfbeis, O. S. *Adv. Mater.* **2010**, *22*, 716−719. (g) Feng, J.; Lei, X.; Wang, S.; Li, S.; Li, Y.; Yang, G. *Adv. Funct. Mater.* **2013**, *23*, 340−345. (h) Cui, Y. J.; Xu, H.; Yue, Y. F.; Guo, Z. Y.; Yu, J. C.; Chen, Z. X.; Gao, J. K.; Yang, Y.; Qian, G. D.; Chen, B. L. *J. Am. Chem. Soc.* **2012**, *134*, 3979−3982. (i) D'Vries, R. F.; Álvarez-García, S.; Snejko, N.; Bausá, L. E.; Gutiérrez-Puebla, E.; de Andrés, A.; Monge, M. A. *J. Mater. Chem. C* **2013**, *1*, 6316−6324.

(5) (a) Ananias, D.; Ferreira, A.; Carlos, L. D.; Rocha, J. *Adv. Mater.* **2003**, *12*, 980−985. (b) Ananias, D.; Carlos, L. D.; Rocha, J. *Opt. Mater.* **2006**, *28*, 582−586.

(6) (a) Ananias, D.; Kostova, M.; Paz, F. A. A.; Ferreira, A.; Carlos, L. D.; Klinowski, J.; Rocha, J. *J. Am. Chem. Soc.* **2004**, *126*, 10410−10417. (b) Ananias, D.; Ferdov, S.; Paz, F. A. A.; Sá Ferreira, R. A.; Ferreira, A.; Geraldes, C. F. G. C.; Carlos, L. D.; Lin, Z.; Rocha, J. *Chem. Mater.* **2008**, *20*, 205−212.

(7) (a) Ananias, D.; Rainho, J. P.; Ferreira, A.; Rocha, J.; Carlos, L. D. *J. Alloys Compd.* **2004**, *374*, 219−222. (b) Ananias, D.; Paz, F. A. A.; Carlos, L. D.; Geraldes, C. F. G. C.; Rocha, J. *Angew. Chem., Int. Ed.* **2006**, *45*, 7938−7942. (c) Ananias, D.; Kostova, M.; Paz, F. A. A.; Neto, A. N. C.; De Moura, R. T.; Malta, O. L.; Carlos, L. D.; Rocha, J. *J. Am. Chem. Soc.* **2009**, *131*, 8620−8626. (d) Ferreira, A.; Ananias, D.; Carlos, L. D.; Morais, C. M.; Rocha, J. *J. Am. Chem. Soc.* **2003**, *125*, 14573−14579.

(8) (a) Suárez, S.; Imbert, D.; Gumy, F.; Piguet, C.; Bünzli, J.-C. G. *Chem. Mater.* **2004**, *16*, 3257−3266. (b) Terazzi, E.; Torelli, S.; Bernardinelli, G.; Rivera, J.-P.; Bénech, J.-M.; Bourgogne, C.; Donnio, B.; Guillon, D.; Imbert, D.; Bünzli, J.-C. G.; Pinto, A.; Piguet, C. *J. Am. Chem. Soc.* **2005**, *127*, 888−903. (c) Kocher, J.; Gummy, F.; Chauvin, A.-S.; Bünzli, J.-C. G. *J. Mater. Chem.* **2007**, *17*, 654−657.

(9) (a) Maczka, M.; Paraguassu, W.; Souza Filho, A. G.; Freire, P. T. C.; Mendes Filho, J.; Hanuza, J. *Phys. Rev. B: Condens. Matter Mater. Phys.* **2008**, *77*, 094137. (b) Gong, C.; Li, Q.; Liu, R.; Hou, Y.; Wang, J.; Dong, X.; Liu, B.; Tan, X.; Liu, J.; Yang, K.; Zou, B.; Cui, T.; Liu, B. *J. Phys. Chem. C* **2014**, *118*, 22739−22745.

(10) Shannon, R. D.; Gier, T. E.; Foris, C. M.; Nelen, J. A.; Appleman, D. E. *Phys. Chem. Miner.* **1980**, *5*, 245−253.

(11) (a) Chicagov, A. V.; Belov, N. V. *Geokhimiya* **1968**, *12*, 1456−1461. (b) Blasse, G.; Bril, A. *J. Inorg. Nucl. Chem.* **1967**, *29*, 2231−2241.

(12) Kottke, T.; Stalke, D. *J. Appl. Cryst.* **1993**, *26*, 615−619.

(13) *APEX2 Data Collection Software*, Version 2012.4; Bruker AXS: Delft, The Netherlands, 2012.

(14) *SAINT+ Data Integration Engine*, Version 8.27b; Bruker AXS: Madison, WI, 2012.

(15) Sheldrick, G. M. *SADABS*, Version 2012/1, Bruker/Siemens Area Detector Absorption Correction Program; Bruker AXS: Madison, WI, 2012.

(16) (a) Sheldrick, G. M. *Acta Crystallogr., Sect. A: Found. Crystallogr.* **2008**, *64*, 112−122. (b) Sheldrick, G. M. *SHELXS-97*, Program for Crystal Structure Solution; University of Göttingen: Göttingen, Germany, 1997.

(17) Sheldrick, G. M. *SHELXL-97*, Program for Crystal Structure Refinement; University of Göttingen: Göttingen, Germany, 1997.

(18) *SAINT+ Data Integration Engine*, Version 8.30c; Bruker AXS: Madison, WI, 2013.

DOI: 10.1021/ja512745y
J. Am. Chem. Soc. 2015, 137, 3051−3058

(19) Sheldrick, G. M. *SHELXT-2014*, Program for Crystal Structure Solution; University of Göttingen: Göttingen, Germany, 2014.
(20) Hübschle, C. B.; Sheldrick, G. M.; Dittrich, B. *J. Appl. Crystallogr.* **2011**, *44*, 1281−1284.
(21) Sheldrick, G. M. *SHELXL*, Version 2014/3, Program for Crystal Structure Refinement; University of Göttingen: Göttingen, Germany, 2014.
(22) Brandenburg, K. *DIAMOND*, Version 3.2f; Crystal Impact GbR: Bonn, Germany, 2010.
(23) *CrystalMaker*, Version 9.0.1; CrystalMaker Software, Ltd.: Yarnton, U.K., 2014.
(24) Sá Ferreira, R. A.; Nobre, S. S.; Granadeiro, C. M.; Nogueira, H. I. S.; Carlos, L. D.; Malta, O. L. *J. Lumin.* **2006**, *121*, 561−567.
(25) (a) Brites, C. D.; Lima, P. P.; Silva, N. J.; Millán, A.; Amaral, V. S.; Palacio, F.; Carlos, L. D. *Nanoscale* **2013**, *5*, 7572−7580. (b) Wei, Y.; Sa, R.; Li, Q.; Wu, K. *Dalton Trans.* **2015**, *44*, 3067−3074.
(26) Canny, B.; Curie, D. Non-Radiative Relaxation of Solids: Different Pathways to the Ground State. In *Advances in Nonradiative Processes in Solids*; Di Bartolo, B., Ed.; Plenum Press: New York, NY, 1991; pp 1−28.
(27) Brites, C. D. S.; Lima, P. P.; Silva, N. J. O.; Millán, A.; Amaral, V. S.; Palacio, F.; Carlos, L. D. *Nanoscale* **2012**, *4*, 4799−4829.
(28) Alencar, M. A. R. C.; Maciel, G. S.; de Araújo, C. B.; Patra, A. *Appl. Phys. Lett.* **2004**, *84*, 4753−4755.
(29) Debasu, M. L.; Ananias, D.; Pastoriza-Santos, I.; Liz-Marzan, L. M.; Rocha, J.; Carlos, L. D. *Adv. Mater.* **2013**, *25*, 4868−4874.
(30) Du, Y.; Liu, T.; Ding, Z.; Han, Q.; Liu, K.; Jiang, J.; Chen, Q.; Feng, B. *IEEE Photonics Technol. Lett.* **2014**, *26*, 1150−1153.
(31) (a) Rodrigues, C. V.; Luz, L. L.; Diogo, J.; Dutra, L.; Junior, S. A.; Malta, O. L.; Gatto, C. C.; Streit, H. C.; Freire, R. O.; Wickleder, C.; Rodrigues, M. O. *Phys. Chem. Chem. Phys.* **2014**, *16*, 14858−14866. (b) Majoul, I.; Jia, Y.; Duden, R. Practical Fluorescence Resonance Energy Transfer or Molecular Nanobioscopy of Living Cells. In *Handbook Of Biological Confocal Microscopy*, 3rd ed.; Pawley, J. B., Ed.; Springer: New York, NY, 2006; pp 788−808.
(32) Fujii, T.; Kodaira, K.; Kawauchi, S.; Tanaka, N.; Yamashita, H.; Anpo, M. *J. Phys. Chem. B* **1997**, *101*, 10631−10637.

DOI: 10.1021/ja512745y
J. Am. Chem. Soc. 2015, 137, 3051−3058